doi: 10.18323/2782-4039-2024-1-67-5

Electrospark modification of the surface of additive VT6 alloy with high-entropy and amorphous electrodes

Samat K. Mukanov*[1], PhD (Engineering), junior researcher
of Scientific-Educational Center of Self-Propagating High-Temperature Synthesis
Pavel A. Loginov[2], PhD (Engineering), senior researcher
of Scientific-Educational Center of Self-Propagating High-Temperature Synthesis
Mikhail I. Petrzhik[3], Doctor of Sciences (Engineering),
professor of Chair of Powder Metallurgy and Functional Coatings,
leading researcher of Scientific-Educational Center of Self-Propagating High-Temperature Synthesis
Evgeny A. Levashov[4], Doctor of Sciences (Engineering), Professor,
Head of Chair of Powder Metallurgy and Functional Coatings,
Head of Scientific-Educational Center of Self-Propagating High-Temperature Synthesis
National University of Science and Technology MISIS, Moscow (Russia)

***E-mail: smukanov@misis.ru**

[1]ORCID: https://orcid.org/0000-0001-6719-6237
[2]ORCID: https://orcid.org/0000-0003-2505-2918
[3]ORCID: https://orcid.org/0000-0002-1736-8050
[4]ORCID: https://orcid.org/0000-0002-0623-0013

Received 23.06.2023 *Accepted 16.11.2023*

Abstract: Unsatisfactory quality of the surface layer of additive products, in particular increased surface roughness, prevents the widespread use of electron beam powder bed fusion (EBPBF). Electrospark treatment (EST) is one of the methods for smoothing and hardening the surface layer. The work shows the possibility of modifying the surface of additive VT6 alloy samples by reactive EST with multicomponent electrodes. For this purpose, the authors used electrodes made of the $Fe_{48}Cr_{15}Mo_{14}Y_2C_{15}B_6$ bulk metallic glass forming alloy and the $FeCoCrNi_2$ high-entropy alloy. Based on the results of scanning electron microscopy, it was identified that after EST, both modified layers have a thickness of about 16 μm. X-ray diffraction phase analysis showed that in the case of treatment with an amorphous electrode they contain carboborides of the Ti(B,C) type, and in the case of treatment with a high-entropy electrode – intermetallic of the Ti_2(Fe,Ni) type. The modified layers have average hardness values of 19 and 10 GPa and elastic modulus of 234 and 157 GPa, respectively, which significantly exceeds the values of these parameters for the EBPBF-grown VT6 alloy. Electric discharge modification of the surface with multicomponent electrodes led to a decrease in roughness by 8...11 times due to the melting of the protrusions and filling of the dimples with the melt to a depth of more than 50 μm. A comparative analysis of the results of tribological tests showed a change in the wear mechanism as a result of EST of the additive VT6 alloy. Wear resistance increased by 4 and 3 orders of magnitude when using electrodes made of a bulk metallic glass and high-entropy alloy, respectively.

Keywords: titanium alloy; electron beam powder bed fusion; surface roughness; smoothing; hardening; wear resistance; electrospark treatment; bulk metallic glass forming alloy; high-entropy alloys.

Acknowledgements: The work was financially supported by the Ministry of Science and Higher Education of the Russian Federation within the state assignment in the sphere of science (project No. 0718-2020-0034).

The paper was written on the reports of the participants of the XI International School of Physical Materials Science (SPM-2023), Togliatti, September 11–15, 2023.

For citation: Mukanov S.K., Loginov P.A., Petrzhik M.I., Levashov E.A. Electrospark modification of the surface of additive VT6 alloy with high-entropy and amorphous electrodes. *Frontier Materials & Technologies*, 2024, no. 1, pp. 49–60. DOI: 10.18323/2782-4039-2024-1-67-5.

INTRODUCTION

Poor surface quality is one of the main factors limiting the development of additive technologies (AT) [1; 2]. Electron beam powder bed fusion (EBPBF), used to grow titanium products allows obtaining good properties in bulk, however, defects (unmelted particles, pores, cracks) are formed on their surface, which reduces surface-sensitive properties, such as wear resistance [3; 4]. Taken together, surface defects determine increased roughness [5; 6], which has a critical impact on the service life and reliability of manufactured products [7]. Currently, to improve the quality of additive surfaces, various post-processing methods are used, which are divided into processing with [8–10], and without [11–13] surface layer removal.

The first group includes methods of mechanical processing and electrochemical processing, which allow obtaining rather smooth surfaces with a roughness of less than 0.5 μm. The latter includes laser processing, and surface modification by deposition of coatings. In particular, in [13], the possibility of using laser polishing of the Inconel 718 nickel alloy was demonstrated, which allows reducing the surface roughness *Ra* from 7.5 to 1 μm. It was shown that laser exposure led to a decrease in grain

size and an increase in microhardness from 345 to 440 HV. The main disadvantage of such methods is uncontrolled heating of the blank part, which leads to bulk recrystallization [14; 15]. The application of electrospark treatment (EST) of EBPBF-grown products is free of this disadvantage, since the supplied energy leads to insignificant heating [16; 17].

The application of electrodes made of multicomponent alloys, such as bulk metallic glass forming alloys (BMG), and so-called high-entropy alloys (HEA), in the reactive EST technology is of particular interest.

Bulk metallic glass forming alloys are based on near-eutectic compositions of multicomponent systems, in which the melt solidifies during deep supercooling with the formation of amorphous or metastable phases [18]. The advantage of these electrodes is their chemical and structural homogeneity, characteristic of metallic glasses, and the near-eutectic composition of low-melting electrodes ensures deep supercooling of the melt, formed during local melting of the electrode, spreading of melt drops over the substrate surface, filling of dimples and obtaining modified surfaces with an amorphous/nanocrystalline structure.

The prospects of using in EST technology of multicomponent cast electrodes with high glass-forming ability produced by vacuum metallurgy, were experimentally shown in [18; 19]. In particular, in [18], $Fe_{48}Cr_{15}Mo_{14}Y_2C_{15}B_6$ and $Fe_{61}Ni_4Cr_3Nb_8Mn_4Si_2B_{18}$ cast electrodes were used to perform EST of substrates made of carbon steel, and VT20 grade titanium alloy (Ti–6.5Al–V–Mo–2Zr). EST with amorphous electrodes allowed increasing the hardness of the VT20 titanium alloy by 3 times, and increasing the wear resistance by 3 orders of magnitude. In [19], as a result of vacuum EST of an AISI 420S steel substrate using a $Fe_{41}Co_7Cr_{15}Mo_{14}C_{15}B_6Y_2$ electrode, a surface with an amorphous structure was obtained. It was noted that the low roughness of the electric discharge surfaces was ensured, due to the formation of melt drops that spread over the substrate surface.

Due to the high configurational entropy of mixing components, HEAs [20] tend to form a structure of a single solid solution. However, it is metastable, and when heated by an electric spark discharge, it experiences decomposition, the products of which, interacting with the substrate elements, can form a modified layer strengthened by intermetallic compounds.

The studies discussed above show that the application of multicomponent electrodes in the EST technology to improve the quality of additive surfaces is promising, but requires additional study.

The purpose of this study is to test multicomponent alloys with high glass-forming ability, and high mixing entropy as electrodes for the reactive EST of the additive VT6 titanium alloy.

METHODS

EBPBF-grown VT6 alloy (Ti–6Al–4V) was used as substrates (cathodes). Table 1 presents the chemical composition of the alloy.

Rod electrodes (anodes), with a diameter of 3 mm made of bulk metallic glass forming $Fe_{48}Cr_{15}Mo_{14}Y_2C_{15}B_6$ alloy, were produced by induction melting followed by casting the melt into a copper mold at an argon pressure of 0.2 atm. Multicomponent electrodes made of high-entropy $FeCoCrNi_2$ alloy powder were produced, by hot pressing (HP) on a DSP-515 SA press (Dr. Fritsch, Germany) in a vacuum, at a temperature of 950 °C, a pressure of 35 MPa, and an isobaric holding for 3 min.

Electrospark treatment was carried out on an Alier-Metal 303 machine in an argon environment, using a vibrating anode holder according to the following mode: current strength – 120 A; pulse duration – 20 μs; voltage – 20 V; pulse energy – 48 mJ; pulse frequency – 3200 Hz.

The kinetics of mass transfer of multicomponent electrodes onto a titanium substrate during EST (specific anode erosion ΔA_i and specific weight gain of the cathode ΔK_i), was measured by the gravimetric method for 5 min on a KERN 770 analytical balance (KERN, Germany) with an accuracy of 10^{-5} g. Measuring of the cathode and anode mass was carried out every minute after EST on an Alier-Metal 303 machine.

X-ray diffraction (XRD) phase analysis was carried out using spectra obtained on a D2 PHASER diffractometer (Bruker AXS, Germany) in monochromatic Cu-Kα ($\lambda K\alpha$=0.15418 nm) radiation in the 2θ angle range from 10° to 120°. Microstructural studies were performed on an S-3400N scanning electron microscope (SEM) (Hitachi High-Technology Corporation, Japan), equipped with a NORAN System 7 X-ray energy-dispersive spectrometer (Thermo Scientific, USA).

Tribological tests were carried out on a Tribometer friction machine (CSM Instruments, Switzerland), at room temperature with reciprocating motion according to the "pin – plate" scheme. A fixed ball with a diameter of 3 mm made of 100Cr6 grade steel (analogous to ShH15) was used as a counterbody. Test conditions: track length is 4 mm, applied load is 1 and 2 N, maximum speed is 5 cm/s. Observation of counterbody wear spot was carried out using an AXIOVERT CA25 optical microscope (ZEISS, Germany) at ×100 magnification. Wear tracks and surface roughness

Table 1. *Composition of the VT6 titanium alloy (Ti–6Al–4V) according to GOST 19807–91*
Таблица 1. *Состав титанового сплава ВТ6 (Ti–6Al–4V) по ГОСТ 19807–91*

Concentration, at. %						
Ti	**Al**	**V**	**O**	**Si**	**Fe**	**Zr**
83.74	10.98	4.08	0.57	0.24	0.24	0.15

were studied using a WYKO NT1100 optical profilometer (Veeco, USA). Mechanical properties (hardness and elastic modulus), were studied using a Nano-HardnessTester instrument (CSM Instruments, Switzerland) at a maximum load of 10 mN.

RESULTS

The surface of the substrates was characterized by a "loose" relief (Fig. 1 a), which was formed by unmelted spherical particles of the original powder with a size of 70...90 μm representing typical defects for EBPBF technology.

The substrate structure was two-phase, and consisted of α and β phases of titanium with lattice parameter of 0.2913 and 0.3152 nm, respectively (Fig. 1 b).

The curves of mass transfer kinetics for both types of electrodes presented in Fig. 2 indicate an increase in the thickness of the electric spark layer throughout the entire duration of treatment (5 min/cm^2). The curves of mass increase of titanium alloy substrates, described by a power function, indicate a low contribution of reverse transfer. The greatest weight gain ($\Delta K_5=5.0\cdot10^{-4}$ g) is observed during treatment with a BMG-electrode. At the same time, the HEA-electrode erosion during treatment of the titanium substrate additive surface was more intense.

Fig. 3 shows images of microstructure of cross-section of the EBPBF-titanium alloy after treatment with a BMG-electrode. The modified layer, about 16 μm thick, has a gradient structure with pronounced dark inclusions.

According to energy dispersive X-ray spectroscopy (EDX) data presented in Table 2, these inclusions are TiC carbide particles. As the distance from the surface increases, the size of the carbide particles increases from 100 to 300 nm. Dark region 3 (Fig. 3 b) at the boundary of the modified layer, and the substrate contains several elements (Ti, Fe, Cr, Mo, Al, Y, C) with a predominance of Ti (51.0 at. %) and corresponds to the zone of primary interaction between the electrode and the substrate.

Images of the titanium substrate microstructure, after treatment with a HEA-electrode are shown in Fig. 4. Treatment of the titanium alloy additive surface with a HEA-electrode also led to the formation of a modified layer 16 μm thick (Fig. 4 a). One can observe that the modified layer has a structure without inclusions compared to the layer formed by a BMG-electrode. This layer is characterized by a high Ti content (60...75 at. %) throughout the entire thickness. EDX (Table 3) showed that the concentration of elements in the surface layer (region 1) and the melt-filled dimples (region 3) is almost the same, which indicates a uniform distribution of elements throughout the entire thickness.

Fig. 4 b shows that, due to the action of electric spark pulses, local melting of both the electrode and the substrate occurred. The resulting melt filled the surface dimples of the substrate. The depth of filling of the dimples with the melt is in the range of 52.3±1.8 μm.

Fig. 5 and Table 4 show the results of XRD phase analysis of modified layers, formed during EST with

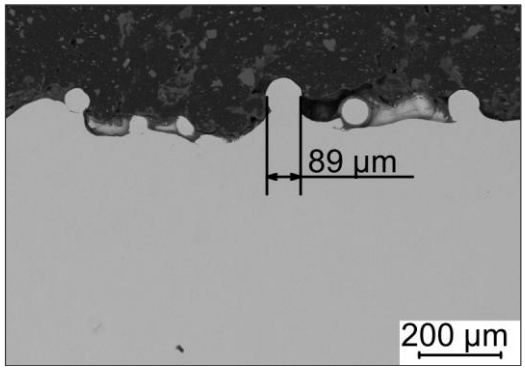

a

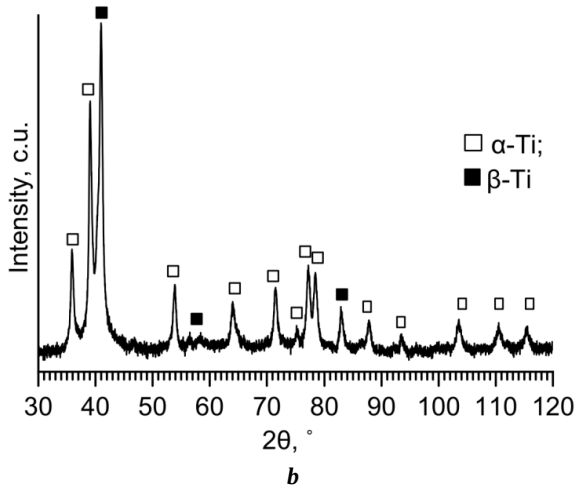

b

Fig. 1. *Cross-section image (**a**) and diffraction pattern (**b**) of a VT6 EBPBF sample in the initial state*
Рис. 1. *Изображение поперечного шлифа (**a**) и дифрактограмма (**b**) СЭЛС-образца ВТ6 в исходном состоянии*

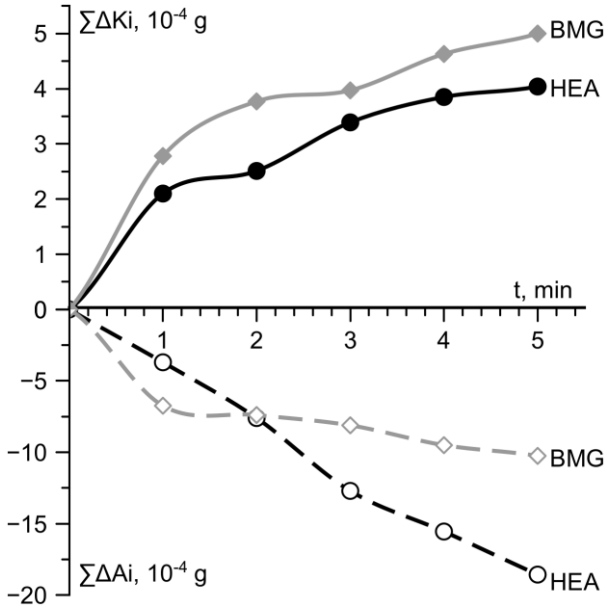

Fig. 2. *Cathode weight gain and anode erosion during EST of a titanium alloy with BMG and HEA electrodes: solid line is substrate weight gain, dashed line is electrode erosion*
Рис. 2. *Привес катода и эрозия анода при ЭИО титанового сплава ОАС- и ВЭС-электродами: сплошная линия – привес массы подложки, пунктирная линия – эрозия электрода*

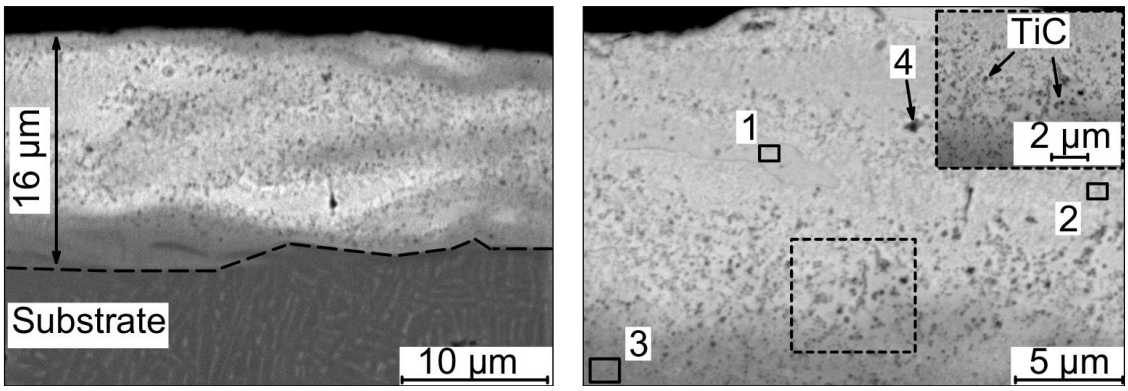

a ***b***

Fig. 3. *SEM image in the backscattered electron (BSE) mode of the cross-section of the VT6 EBPBF sample after EST with a BMG-electrode (**a**); EDX analysis area (inset contains a magnified image of the selected area) (**b**)*
Рис. 3. *РЭМ-изображение в режиме обратно отраженных электронов (BSE) поперечного шлифа СЭЛС-образца ВТ6 после ЭИО ОАС-электродом (**а**); области ЭДС-анализа (на вставке увеличенное изображение выделенной области) (**b**)*

Table 2. *EDX analysis results of areas shown at Fig. 3 b*
Таблица 2. *Результаты ЭДС-анализа областей, показанных на рис. 3 b*

No.	Concentration, at. %							
	Fe	C	Ti	Cr	Mo	Al	V	Y
1	33.4	24.4	19.6	10.7	8.0	2.7	0.9	0.4
2	32.7	25.5	19.0	10.5	9.1	2.0	0.8	0.4
3	15.6	19.3	51.0	5.4	4.3	4.0	–	0.4
4	16.1	35.4	34.1	6.0	5.8	1.3	–	–

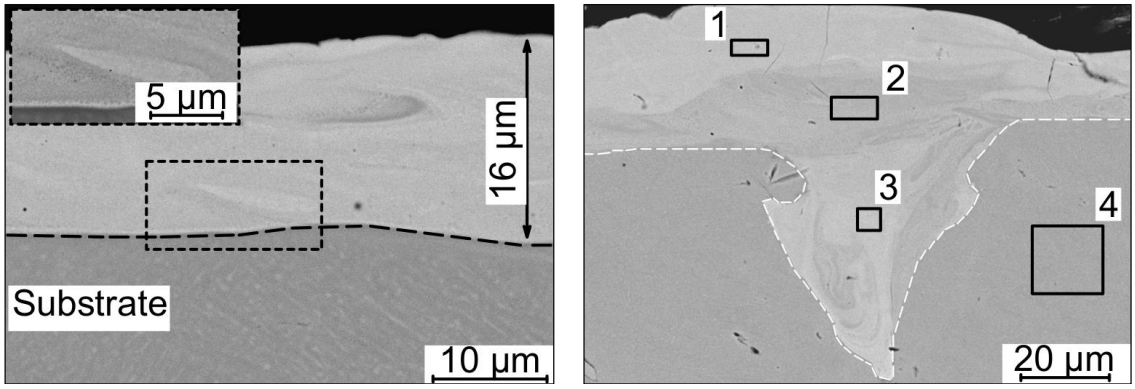

a *b*

Fig. 4. *SEM images in the backscattered electron (BSE) mode: modified layer of the VT6 EBPBF sample after EST with a HEA-electrode (insert contains a magnified image of the selected area) (**a**); a deep dimple filled with the melt during EST (**b**)*
Рис. 4. *РЭМ-изображения в режиме обратно отраженных электронов (BSE): модифицированный слой СЭЛС-образца ВТ6 после ЭИО ВЭС-электродом (на вставке увеличенное изображение выделенной области) (**а**); глубокая впадина, заполненная расплавом при ЭИО (**b**)*

Table 3. *EDX analysis results of areas shown at Fig. 4 b*
Таблица 3. *Результаты ЭДС-анализа областей, показанных на рис. 4 b*

No.	Concentration, at. %						
	Ti	Ni	Fe	Al	Cr	Co	V
1	59.4	10.8	8.3	7.1	6.1	5.5	2.8
2	74.5	4.7	4.0	8.7	2.4	2.2	3.6
3	65.0	8.9	6.8	7.8	4.3	4.2	3.0
4	86.3	–	–	9.5	–	–	4.2

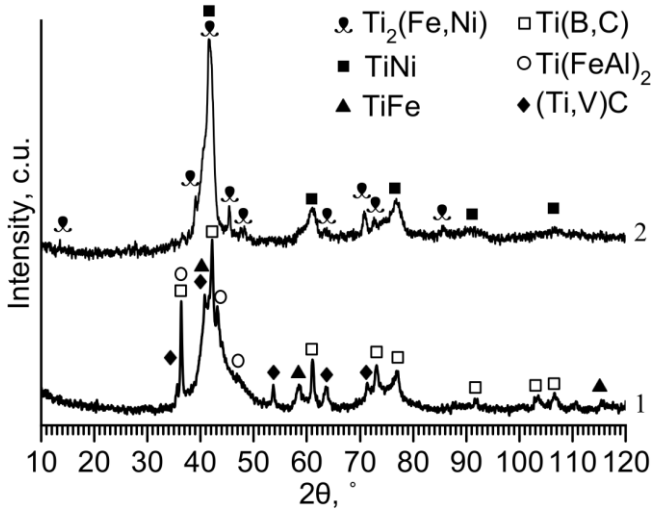

Fig. 5. *X-ray diffraction pattern of the VT6 EBPBF sample after EST with an electrode: 1 – $Fe_{48}Cr_{15}Mo_{14}Y_2C_{15}B_6$ BMG-electrode; 2 – $FeCoCrNi_2$ HEA-electrode*
Рис. 5. *Дифрактограмма СЭЛС-образца ВТ6 после ЭИО электродом: 1 – ОАС-электрод $Fe_{48}Cr_{15}Mo_{14}Y_2C_{15}B_6$; 2 – ВЭС-электрод $FeCoCrNi_2$*

Table 4. *Phase composition of samples subjected to EST*
Таблица 4. *Фазовый состав образцов, подвергнутых ЭИО*

Electrode used at EST	Phase	Portion, wt. %	Lattice parameter, nm		
			(a)	(b)	(c)
$Fe_{48}Cr_{15}Mo_{14}Y_2C_{15}B_6$	Ti(B,C)	44.8	0.8558	–	–
	$Ti(FeAl)_2$	27.5	0.4920	–	0.7988
	(Ti,V)C	14.6	0.2904	–	0.4640
	TiFe	13.1	0.3153	–	–
$FeCoCrNi_2$	$Ti_2(Fe,Ni)$	60.1	1.1296	–	–
	TiNi	39.9	0.3039	–	–

multicomponent electrodes. At processing with a BMG-electrode, chemically active titanium interacted with the electrode elements resulting in the formation of cubic phases: carbides and intermetallics. According to the EDX data (Table 2), the carbide particles contain Ti and C. Considering that the EDX resolution does not allow identifying boron contained in the BMG-electrode, these particles (Fig. 3 b) are probably carboborides of the Ti(B,C) type. The interaction of the Al and V substrate elements with the electrode leading to the formation of hexagonal $Ti(FeAl)_2$ and (Ti,V)C phases was also discovered.

The structure of the layer modified by the HEA-electrode consists of two phases; the diffraction peaks in the diffraction pattern can be attributed to the $Ti_2(Fe,Ni)$ and TiNi cubic phases. One should note that there is a halo in both diffraction patterns, confirming the formation of an amorphous phase during EST, as was found in [18], which is more pronounced for the sample treated with a BMG-electrode.

Table 5 presents the results of studying the surface topography of the modified layers. The initial titanium sample additive surface was characterized by a high roughness (*Ra*) of 38.75±3.00 μm. One can see that treatment with multicomponent electrodes noticeably reduces the values of the arithmetic average of profile height deviations (*Ra*) and maximum peak to valley height of the profile (*Rz*) compared to the additive surface of the original titanium alloy. The minimum surface roughness of 3.53±0.31 μm is observed when processed with a BMG-electrode, and is probably determined by the high fluidity of the electrode material.

The effect of the titanium alloy EST, with multicomponent electrodes on the tribological and mechanical properties can be traced in Fig. 6 and 7. As one can see in Fig. 6 a, the starting friction coefficient (FC) for the titanium substrate is 0.23, and it increases monotonically to 0.33 at the end of the test. When the counterbody slides over the layer formed by a BMG-electrode, three stages can be seen: up to 1000 cycles, a low FC (0.09...0.12) remains unchanged; during the breaking-in period (up to 1500 cycles), a FC monotonically increases from 0.15 to 0.32, and the steady-state friction coefficient reaches 0.36. Increasing the applied load from 1 to 2 N on the steel ball led to an increase in FC up to 0.39. When testing a layer formed by a HEA-electrode, the starting FC is the highest (0.25), and after 500 cycles, a more significant increase in FC up to 0.48 is observed.

The results of measuring mechanical properties (Fig. 6 b, Table 6) showed that EST leads to an increase in both hardness (4 times for BMG and 2 times for HEA) and elastic modulus (1.7 times for BMG and 1.2 times for HEA) of the titanium alloy. The average hardness values of the layers formed by the BMG- and HEA-electrodes were 18.7±2.5 and 10.0±0.9 GPa, respectively.

To study the nature of wear of the samples, the areas of tribocontact on the counterbody, and the sample were studied (Fig. 7). Fig. 7 a–c shows the wear spot of the steel ball. The adhering of wear debris to the ball, while maintaining its spherical shape, confirms the higher hardness of the counterbody compared to the titanium alloy.

The presence of deep grooves in the counterbody wear spot (Fig. 7 b, 7 c) indicates a greater hardness of the layer formed on VT6, during processing with multicomponent electrodes compared to the counterbody material.

The reduced wear of the untreated titanium alloy is the highest (10^{-3} $mm^3/(N \cdot m)$). After treating the titanium alloy with a BMG-electrode, no wear groove was detected at a load of 1 N, which corresponds to a reduced wear value of less than 10^{-7} $mm^3/(N \cdot m)$. Therefore, to test samples with a modified layer, the load was increased up to 2 N. With an increase in the applied load from 1 to 2 N (Table 6), the wear of the steel counterbody increased from 3.18 to $3.84 \cdot 10^{-5}$ $mm^3/(N \cdot m)$, while the wear of the modified layer did not change ($<10^{-7}$ $mm^3/(N \cdot m)$).

DISCUSSION

As known [21], erosion of electrodes during an electric spark discharge depends on a number of factors: density, heat capacity, specific heat of fusion, thermal coefficient of electrical resistance, etc. Their porosity has a great influence on the erosion resistance of electrodes. Previously [22], to increase erosion and accelerate mass transfer during EST, electrodes with increased porosity (5–10 %) produced by powder metallurgy methods were used. In this study, HEA-electrodes were produced using HP technology,

Table 5. *Surface roughness of the VT6 alloy EBPBF samples before and after EST*
Таблица 5. *Шероховатость поверхности СЭЛС-образцов сплава ВТ6 до и после ЭИО*

Sample	*Ra*, μm	*Rz*, μm
EBPBF of the VT6 alloy	38.75±3.00	221.72±38.00
EST with a BMG-electrode	3.53±0.31	36.19±5.00
EST with a HEA-electrode	4.66±0.28	37.26±3.98

Table 6. *Tribological and mechanical properties of samples*
Таблица 6. *Трибологические и механические свойства образцов*

Sample	I, 10^{-5}·mm^3/(N·m)		FC (final)	H, GPa	E, GPa
	of a sample	of a counterbody			
EBPBF of the VT6 alloy	159.60	sticking	0.33	4.7±0.3	136±7
+ EST with a BMG-electrode	<10^{-7}	3.18	0.36	18.7±2.5	234±32
+ EST with a BMG-electrode*	<10^{-7}	3.84	0.39		
+ EST with a HEA-electrode*	3.24	3.33	0.48	10.0±0.9	157±15

Note. *******Applied load is 2 N.*
Примечание. *******Приложенная нагрузка – 2 Н.*

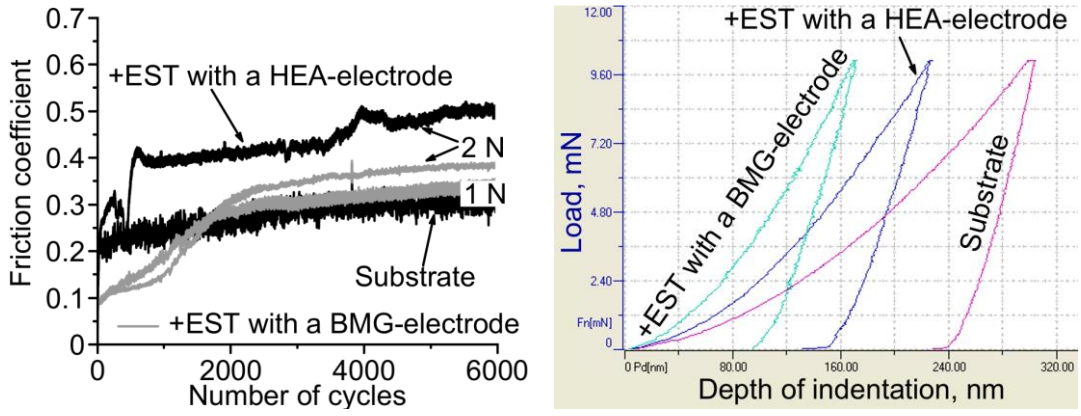

a ***b***

Fig. 6. *Experimental dependences of the friction coefficient on the number of cycles* ***(a)*** *and nanoindentation curves* ***(b)***
Рис. 6. *Экспериментальные зависимости коэффициента трения от количества циклов* ***(а)*** *и кривые наноиндентирования* ***(b)***

so large erosion values (Fig. 2) can be explained by the presence of pores in them (porosity is 3.8±0.2 %). The increase in the cathode weight gain (ΔK_5=5.0·10^{-4} g) during treatment with a BMG-electrode, can be explained by a lower melting point, higher ability melt to undercooling (ΔT=38 °C) and better fluidity [18].

Modified layers, formed during EST with multicomponent electrodes, have a gradient or layered structure. Probably, such a structure is associated with the mixing of melt droplets, containing substrate and electrode elements, as a result of repeated exposure to pulsed electric spark discharges. During EST, spark pulses with a duration of 20 μs, cause local heating and melting of the anode and cathode, ensuring their chemical and diffusion interaction leading to reaction phase formation. Heat removal by the metal substrate provides a high quenching rate of melt (10^5–10^7) K/s [18; 23], which leads to surface layer hardening.

The modified layer produced by EST, with an amorphous $Fe_{48}Cr_{15}Mo_{14}Y_2C_{15}B_6$ electrode significantly differs in structure from the layer produced by EST with

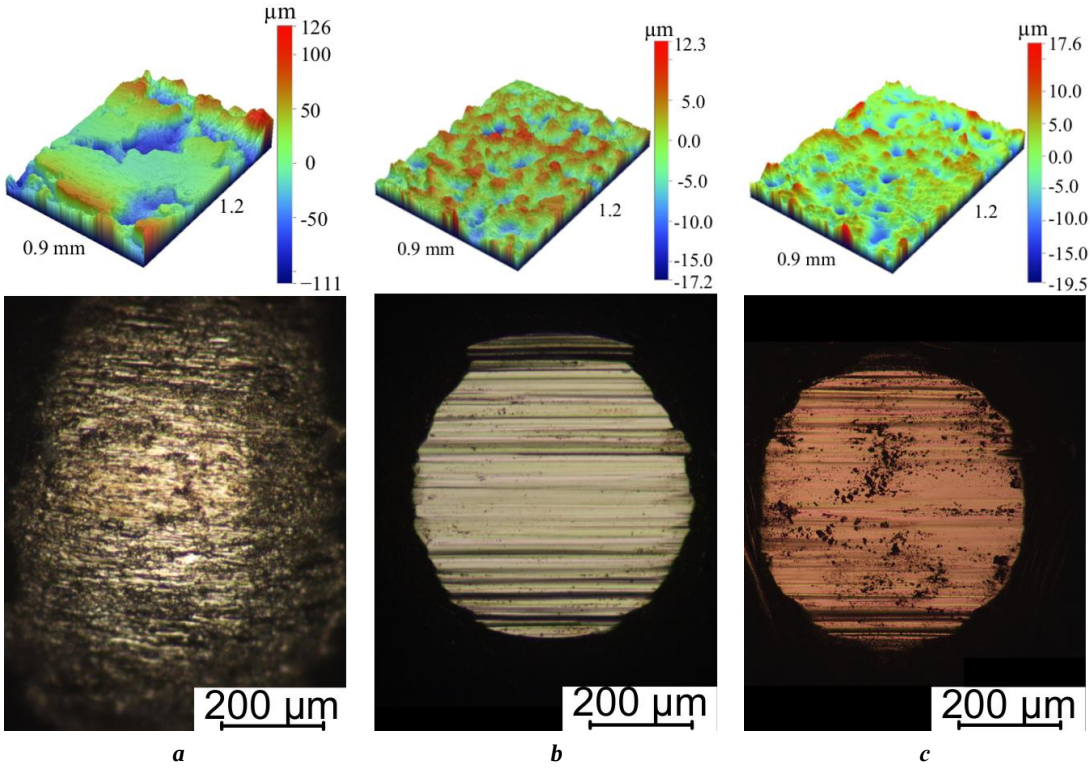

Fig. 7. *Micrographs of counterbodies and 3D-images of wear tracks after tribotestins of samples: the VT6 alloy tested at the load of 1 N* ***(a)****; of modified layers formed with BMG-electrode* ***(b)****; HEA-electrode* ***(c)*** *(both tested at 2 N)*

Рис. 7. *Микрофотографии контртел и 3D-изображения дорожек износа образцов после трибоиспытаний: исходный сплав ВТ6 (при нагрузке 1 Н)* ***(a)****; модифицированные слои, сформированные: ОАС-электродом* ***(b)****; ВЭС-электродом* ***(c)*** *(оба при нагрузке 2 Н)*

a $FeCoCrNi_2$ electrode. A characteristic feature of the first one (Fig. 3) is its gradient structure; the size of Ti(B,C) carboboride particles varies within 100...500 nm, with larger particles located further from the surface. When treated with a $FeCoCrNi_2$ electrode, a layer is formed with a predominant proportion of the $Ti_2(Fe,Ni)$ intermetallic. The increased Ti content (Table 3) in this modified layer is caused by the processing electrode composition. The amorphous electrode composition, in contrast to HEA, contains active metalloids (carbon, boron), which react with Ti forming new phases (in particular, Ti(B,C)).

As can be observed from Table 5, the roughness of modified layers, just as the starting FC (Fig. 6 a), was much lower than that of the additive surface of the original EBPBF VT6.

As shown in Fig. 7 b, 7 c, in the area of contact of the counterbody with the modified layers, the wear mechanism changes. It is observed not the adhering of wear products, but the formation of deep grooves, which is more pronounced after testing a sample treated with a BMG-electrode, the structure of which contains TiC carbide particles (Fig. 3). This indicates that the counterbody is scratched by solid particles crumbled from the modified layer of the sample at the initial stage of testing, where the abrasive wear mechanism may predominate. Wear of a sample treated with a HEA-electrode, occurs both through crumbling at the beginning of the test and through further grinding of particles of the solid and brittle $Ti_2(Fe,Ni)$ phase, which leads to smoothing of the counterbody central part by wear products. In this case, the monotonic increase in the friction coefficient up to 0.48, with sliding counterbody occurs due to an increase in the contact area.

Based on the comprehensive tribological study, Fig. 8 shows a schematic representation of the wear mechanism of the original titanium alloy, and samples with modified layers. Reduced FC (0.33) when the counterbody slides along the untreated sample surface is probably caused by the occurrence of a solid-phase reaction of chemically active Ti, with the counterbody ShH15 steel (100Cr6) material. As a result of this sliding of the ball, wear products adhere to its surface (Fig. 7 a). Compaction of wear products under the load, leads to the tribolayer formation in the contact zone providing a reduced friction coefficient.

Increasing the load up to 2 N, when testing a layer after treatment with a BMG-electrode, practically, does not lead to a change in the final friction coefficient (Table 6). This indicates that the wear of this layer during the entire test occurred according to the same mechanism. In this case, an increase in the counterbody wear is observed, but the wear of the modified layer remains unchanged.

Comparing the XRD results with tribological tests, one can conclude that the increase in the wear resistance of the titanium sample treated with a BMG-electrode by 4 orders of magnitude is caused by the formation of Ti(B,C) carboboride. In the case of treatment with a HEA-electrode, despite the high volume fraction of $Ti_2(Fe,Ni)$, the modified layer has a rather high reduced wear value of $3.24 \cdot 10^{-5}$ $mm^3/(N \cdot m)$ compared to the surface treated with

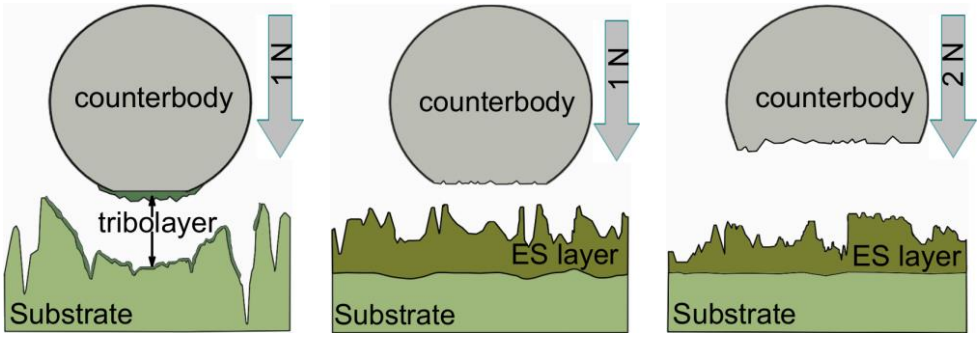

Fig. 8. *Schematic diagram of the wear mechanism of samples before and after EST*
Рис. 8. *Схематическое изображение механизма износа образцов до и после ЭИО*

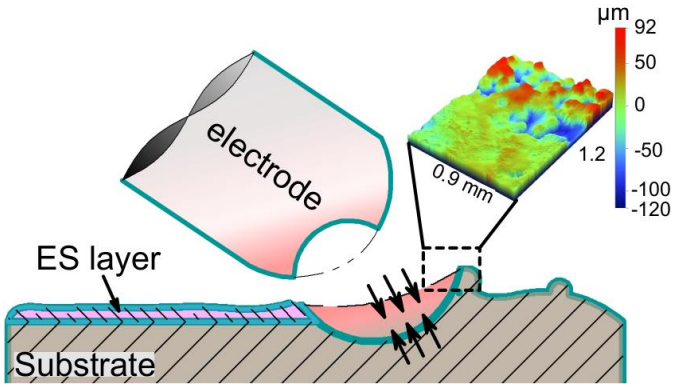

Fig. 9. *Scheme and 3D-image of the surface of the VT6 EBPBF sample after EST with multicomponent electrodes*
Рис. 9. *Схема и 3D-изображение поверхности СЭЛС-образца ВТ6 после ЭИО многокомпонентными электродами*

a BMG-electrode. Thus, the phase composition and microstructure of the modified layers correlate with mechanical and tribological characteristics. The presence of high-hardness phases (Ti(B,C), Ti_2(Fe,Ni)) in the modified layers, in combination with a fine-crystalline structure, led to a significant increase in hardness and elastic modulus compared to the VT6 alloy.

Fig. 9 presents the scheme for smoothing the additive surface of a titanium alloy (substrate). Based on the study of the structure and morphology of the additive sample surface before (Fig. 1) and after EST (Fig. 3, 4), one can assume that when processing the EBPBF sample with multicomponent electrodes, local melting of the protrusions on their surface occurs with the formation of a melt consisting of electrode and substrate elements. This melt spreads over the surface and fills dimples more than 50 μm deep. Thus, the shown in table 5 decrease in the average surface roughness *Ra* by 8 and 11 times for the HEA and BMG electrodes, respectively, can be explained.

CONCLUSIONS

1. Electrospark treatment of additive surface of the titanium alloy with electrodes made of multicomponent alloys, led to the formation of modified layers about 16 μm thick with a submicron structure. When treated with an amorphous electrode, a gradient structure layer is formed, the size of Ti(B,C) carboboride particles varies within 100...500 nm with larger particles located further from the surface.

2. The results of comparative tribological tests of an EBPBF sample with modified layers showed that EST with multicomponent electrodes allows increasing the wear resistance of a titanium alloy. It has been found that an increase by 4 orders of magnitude in the wear resistance of EBPBF samples of titanium alloy, treated with an amorphous electrode, is associated with the formation of Ti(B,C) carboboride in the surface layer due to the interaction of the chemically active melt with the substrate.

3. The results of studying the mechanical properties showed, that EST leads to an increase in both the hardness (2 and 4 times) and the elastic modulus (1.2 and 1.7 times) of the VT6 alloy when treated with high-entropy, and amorphous electrodes, respectively. The quenching of melt droplets with the formation of hard and wear-resistant intermetallics or carboborides plays a key role in the hardening of modified layers during EST.

4. It has been demonstrated that during EST with multicomponent electrodes, a melt is formed, which spreads over the titanium alloy surface filling dimples more than 50 μm deep, which leads to a decrease in surface roughness by 8 and 11 times for the HEA and BMG electrodes, respectively.

REFERENCES

1. Murr L.E., Gaytan S.M., Ceylan A. et al. Characterization of titanium aluminide alloy components fabricated by additive manufacturing using electron beam melting. *Acta Materialia*, 2010, vol. 58, no. 5, pp. 1887–1894. DOI: 10.1016/j.actamat.2009.11.032.
2. Leary M. Surface roughness optimisation for selective laser melting (SLM): Accommodating relevant and irrelevant surfaces. *Laser Additive Manufacturing: Materials, Design, Technologies and Applications*. Sawston, Woodhead Publishing, 2017, pp. 99–118. DOI: 10.1016/B978-0-08-100433-3.00004-X.
3. Karlsson J., Snis A., Engqvist H., Lausmaa J. Characterization and comparison of materials produced by Electron Beam Melting (EBM) of two different Ti–6Al–4V powder fractions. *Journal of Materials Processing Technology*, 2013, vol. 213, no. 12, pp. 2109–2118. DOI: 10.1016/j.jmatprotec.2013.06.010.
4. Calignano F., Manfredi D., Ambrosio E.P. et al. Overview on Additive Manufacturing Technologies. *Proceedings of the IEEE*, 2017, vol. 105, no. 4, pp. 593–612. DOI: 10.1109/JPROC.2016.2625098.
5. Nasab M.H., Gastaldi D., Lecis N.F., Vedani M. On morphological surface features of the parts printed by selective laser melting (SLM). *Additive Manufacturing*, 2018, vol. 24, pp. 373–377. DOI: 10.1016/j.addma.2018.10.011.
6. Leuders S., Thöne M., Riemer A., Niendorf T., Tröster T., Richard H.A., Maier H.J. On the mechanical behaviour of titanium alloy TiAl6V4 manufactured by selective laser melting: Fatigue resistance and crack growth performance. *International Journal of Fatigue*, 2013, vol. 48, pp. 300–307. DOI: 10.1016/j.ijfatigue.2012.11.011.
7. Fé-Perdomo I.L., Ramos-Grez J., Mujica R., Rivas M. Surface roughness Ra prediction in Selective Laser Melting of 316L stainless steel by means of artificial intelligence inference. *Journal of King Saud University - Engineering Sciences*, 2023, vol. 35, no. 2, pp. 148–156. DOI: 10.1016/j.jksues.2021.03.002.
8. Asfandiyarov R.N., Raab G.I., Gunderov D.V., Aksenov D.A., Raab A.G., Gunderova S.D., Shishkunova M.A. Roughness and microhardness of UFG grade 4 titanium under abrasive-free ultrasonic finishing. *Frontier Materials & Technologies*, 2022, no. 3-1, pp. 41–49. DOI: 10.18323/2782-4039-2022-3-1-41-49.
9. Bagehorn S., Wehr J., Maier H.J. Application of mechanical surface finishing processes for roughness reduction and fatigue improvement of additively manufactured Ti-6Al-4V parts. *International Journal of Fatigue*, 2017, vol. 102, pp. 135–142. DOI: 10.1016/j.ijfatigue.2017.05.008.
10. Tan K.L., Yeo S.H. Surface modification of additive manufactured components by ultrasonic cavitation abrasive finishing. *Wear*, 2017, vol. 378-379, pp. 90–95. DOI: 10.1016/j.wear.2017.02.030.
11. Yasa E., Kruth J.-P. Microstructural investigation of Selective Laser Melting 316L stainless steel parts exposed to laser re-melting. *Procedia Engineering*, 2011, vol. 19, pp. 389–395. DOI: 10.1016/j.proeng.2011.11.130.
12. Zhang Baicheng, Zhu Lin, Liao Hanlin, Coddet C. Improvement of surface properties of SLM parts by atmospheric plasma spraying coating. *Applied Surface Science*, 2012, vol. 263, pp. 777–782. DOI: 10.1016/j.apsusc.2012.09.170.
13. Fang Zhihao, Lu Libin, Chen Longfei, Guan Yingchun. Laser Polishing of Additive Manufactured Superalloy. *Procedia CIRP*, 2018, vol. 71, pp. 150–154. DOI: 10.1016/j.procir.2018.05.088.
14. Barile C., Casavola C., Pappalettera G., Renna G. Advancements in Electrospark Deposition (ESD) Technique: A Short Review. *Coatings*, 2022, vol. 12, no. 10, article number 1536. DOI: 10.3390/coatings12101536.
15. Wang De, Deng Shaojun, Chen Hui, Chi Changtai, Hu Dean, Wang Wengin, He Wen, Liu Xiubo. Microstructure and properties of TiC particles planted on single crystal superalloy by electrospark discharging. *Surface and Coatings Technology*, 2023, vol. 461, article number 129438. DOI: 10.1016/j.surfcoat.2023.129438.
16. Liu Xiao-Qin, Zhang Yu-Xing, Wang Xiao-Rong, Wang Zhao-Qin, He Peng. Microstructure and corrosion properties of AlCrxNiCu0.5Mo (x = 0, 0.5, 1.0, 1.5, 2.0) high entropy alloy coatings on Q235 steel by electrospark – Computer numerical control deposition. *Materials Letters*, 2021, vol. 292, article number 129642. DOI: 10.1016/j.matlet.2021.129642.
17. Mukanov S.K., Baskov F.A., Petrzhik M.I., Levashov E.A. Electro-spark treatment with low-melting Al–Si and Al–Ca electrodes in order to improve wear and oxidation resistance of EP741NP alloy prepared by selective laser melting. *Metallurgist*, 2022, vol. 66, no. 3, pp. 317–326. DOI: 10.1007/s11015-022-01331-0.
18. Petrzhik M., Molokanov V., Levashov E. On conditions of bulk and surface glass formation of metallic alloys. *Journal of Alloys and Compounds*, 2017, vol. 707, pp. 68–72. DOI: 10.1016/j.jallcom.2016.12.293.
19. Sheveyko A.N., Kuptsov K.A., Antonyuk M.N., Bazlov A.I., Shtansky D.V. Electro-spark deposition of amorphous Fe-based coatings in vacuum and in argon controlled by surface wettability. *Materials Letters*, 2022, vol. 318, article number 132195. DOI: 10.1016/j.matlet.2022.132195.
20. Mukanov S., Loginov P., Fedotov A., Bychkova M., Antonyuk M., Levashov E. The Effect of Copper on the Microstructure, Wear and Corrosion Resistance of CoCrCuFeNi High-Entropy Alloys Manufactured by Powder Metallurgy. *Materials*, 2023, vol. 16, no. 3, article number 1178. DOI: 10.3390/ma16031178.
21. Gitlevich A.E., Mikhaylov V.V., Parkanskiy N.Ya., Revutskiy V.M. *Elektroiskrovoe legirovanie metallicheskikh poverkhnostey* [Electric-Spark Alloying of Metal Surfaces]. Kishinev, Shtiintsa Publ., 1985. 196 p.
22. Levashov E.A., Merzhanov A.G., Shtansky D.V. Advanced Technologies, Materials and Coatings Developed in Scientific-Educational Center of SHS. *Galvanotechnik*, 2009, vol. 100, no. 9, pp. 2102–2114. EDN: MWXQPL.
23. Zhao Wang, Su Hao, He Weifeng, Wang Xiaorong, Cui Xiaoyu, Luo Sihai. Defect Control of Electro-spark Deposition WC–Co Coatings via Adjusting Pulse Energy and Deposited Layer Number. *Journal of Materials Engineering and Performance*, 2023, vol. 32, pp. 1402–1411. DOI: 10.1007/s11665-022-07204-6.

СПИСОК ЛИТЕРАТУРЫ

1. Murr L.E., Gaytan S.M., Ceylan A. et al. Characterization of titanium aluminide alloy components fabricated by additive manufacturing using electron beam melting // Acta Materialia. 2010. Vol. 58. № 5. P. 1887–1894. DOI: 10.1016/j.actamat.2009.11.032.
2. Leary M. Surface roughness optimisation for selective laser melting (SLM): Accommodating relevant and irrelevant surfaces // Laser Additive Manufacturing: Materials, Design, Technologies and Applications. Sawston: Woodhead Publishing, 2017. P. 99–118. DOI: 10.1016/B978-0-08-100433-3.00004-X.
3. Karlsson J., Snis A., Engqvist H., Lausmaa J. Characterization and comparison of materials produced by Electron Beam Melting (EBM) of two different Ti–6Al–4V powder fractions // Journal of Materials Processing Technology. 2013. Vol. 213. № 12. P. 2109–2118. DOI: 10.1016/j.jmatprotec.2013.06.010.
4. Calignano F., Manfredi D., Ambrosio E.P. et al. Overview on Additive Manufacturing Technologies // Proceedings of the IEEE. 2017. Vol. 105. № 4. P. 593–612. DOI: 10.1109/JPROC.2016.2625098.
5. Nasab M.H., Gastaldi D., Lecis N.F., Vedani M. On morphological surface features of the parts printed by selective laser melting (SLM) // Additive Manufacturing. 2018. Vol. 24. P. 373–377. DOI: 10.1016/j.addma.2018.10.011.
6. Leuders S., Thöne M., Riemer A., Niendorf T., Tröster T., Richard H.A., Maier H.J. On the mechanical behaviour of titanium alloy TiAl6V4 manufactured by selective laser melting: Fatigue resistance and crack growth performance // International Journal of Fatigue. 2013. Vol. 48. P. 300–307. DOI: 10.1016/j.ijfatigue.2012.11.011.
7. Fé-Perdomo I.L., Ramos-Grez J., Mujica R., Rivas M. Surface roughness Ra prediction in Selective Laser Melting of 316L stainless steel by means of artificial intelligence inference // Journal of King Saud University - Engineering Sciences. 2023. Vol. 35. № 2. P. 148–156. DOI: 10.1016/j.jksues.2021.03.002.
8. Асфандияров Р.Н., Рааб Г.И., Гундеров Д.В., Аксенов Д.А., Рааб А.Г., Гундерова С.Д., Шишкунова М.А. Шероховатость и микротвердость ультрамелкозернистого титана Grade 4, подвергнутого безабразивной ультразвуковой финишной обработке // Frontier Materials & Technologies. 2022. № 3-1. С. 41–49. DOI: 10.18323/2782-4039-2022-3-1-41-49.
9. Bagehorn S., Wehr J., Maier H.J. Application of mechanical surface finishing processes for roughness reduction and fatigue improvement of additively manufactured Ti-6Al-4V parts // International Journal of Fatigue. 2017. Vol. 102. P. 135–142. DOI: 10.1016/j.ijfatigue.2017.05.008.
10. Tan K.L., Yeo S.H. Surface modification of additive manufactured components by ultrasonic cavitation abrasive finishing // Wear. 2017. Vol. 378-379. P. 90–95. DOI: 10.1016/j.wear.2017.02.030.
11. Yasa E., Kruth J.-P. Microstructural investigation of Selective Laser Melting 316L stainless steel parts exposed to laser re-melting // Procedia Engineering. 2011. Vol. 19. P. 389–395. DOI: 10.1016/j.proeng.2011.11.130.
12. Zhang Baicheng, Zhu Lin, Liao Hanlin, Coddet C. Improvement of surface properties of SLM parts by atmospheric plasma spraying coating // Applied Surface Science. 2012. Vol. 263. P. 777–782. DOI: 10.1016/j.apsusc.2012.09.170.
13. Fang Zhihao, Lu Libin, Chen Longfei, Guan Yingchun. Laser Polishing of Additive Manufactured Superalloy // Procedia CIRP. 2018. Vol. 71. P. 150–154. DOI: 10.1016/j.procir.2018.05.088.
14. Barile C., Casavola C., Pappalettera G., Renna G. Advancements in Electrospark Deposition (ESD) Technique: A Short Review // Coatings. 2022. Vol. 12. № 10. Article number 1536. DOI: 10.3390/coatings12101536.
15. Wang De, Deng Shaojun, Chen Hui, Chi Changtai, Hu Dean, Wang Wengin, He Wen, Liu Xiubo. Microstructure and properties of TiC particles planted on single crystal superalloy by electrospark discharging // Surface and Coatings Technology. 2023. Vol. 461. Article number 129438. DOI: 10.1016/j.surfcoat.2023.129438.
16. Liu Xiao-Qin, Zhang Yu-Xing, Wang Xiao-Rong, Wang Zhao-Qin, He Peng. Microstructure and corrosion properties of AlCrxNiCu0.5Mo (x = 0, 0.5, 1.0, 1.5, 2.0) high entropy alloy coatings on Q235 steel by electrospark – Computer numerical control deposition // Materials Letters. 2021. Vol. 292. Article number 129642. DOI: 10.1016/j.matlet.2021.129642.
17. Муканов С.К., Басков Ф.А., Петржик М.И., Левашов Е.А. Электроискровая обработка легкоплавкими электродами Al–Si И Al–Ca для повышения стойкости к износу и окислению сплава ЭП741НП, полученного селективным лазерным сплавлением // Металлург. 2022. № 3. С. 70–77. DOI: 10.52351/00260827_2022_03_70.
18. Petrzhik M., Molokanov V., Levashov E. On conditions of bulk and surface glass formation of metallic alloys // Journal of Alloys and Compounds. 2017. Vol. 707. P. 68–72. DOI: 10.1016/j.jallcom.2016.12.293.
19. Sheveyko A.N., Kuptsov K.A., Antonyuk M.N., Bazlov A.I., Shtansky D.V. Electro-spark deposition of amorphous Fe-based coatings in vacuum and in argon controlled by surface wettability // Materials Letters. 2022. Vol. 318. Article number 132195. DOI: 10.1016/j.matlet.2022.132195.
20. Mukanov S., Loginov P., Fedotov A., Bychkova M., Antonyuk M., Levashov E. The Effect of Copper on the Microstructure, Wear and Corrosion Resistance of CoCrCuFeNi High-Entropy Alloys Manufactured by Powder Metallurgy // Materials. 2023. Vol. 16. № 3. Article number 1178. DOI: 10.3390/ma16031178.
21. Гитлевич А.Е., Михайлов В.В., Парканский Н.Я., Ревуцкий В.М. Электроискровое легирование металлических поверхностей. Кишинев: Штиинца, 1985. 196 с.
22. Levashov E.A., Merzhanov A.G., Shtansky D.V. Advanced Technologies, Materials and Coatings Developed in Scientific-Educational Center of SHS // Galvanotechnik. 2009. Vol. 100. № 9. P. 2102–2114. EDN: MWXQPL.
23. Zhao Wang, Su Hao, He Weifeng, Wang Xiaorong, Cui Xiaoyu, Luo Sihai. Defect Control of Electro-spark Deposition WC–Co Coatings via Adjusting Pulse Energy and Deposited Layer Number // Journal of Materials Engineering and Performance. 2023. Vol. 32. P. 1402–1411. DOI: 10.1007/s11665-022-07204-6.

Электроискровое модифицирование поверхности аддитивного сплава ВТ6 высокоэнтропийным и аморфным электродами

Муканов Самат Куандыкович*[*1], кандидат технических наук, младший научный сотрудник научно-учебного центра самораспространяющегося высокотемпературного синтеза
Логинов Павел Александрович[2], кандидат технических наук, старший научный сотрудник научно-учебного центра самораспространяющегося высокотемпературного синтеза
Петржик Михаил Иванович[3], доктор технических наук, профессор кафедры порошковой металлургии и функциональных покрытий, ведущий научный сотрудник научно-учебного центра самораспространяющегося высокотемпературного синтеза
Левашов Евгений Александрович[4], доктор технических наук, профессор, заведующий кафедрой порошковой металлургии и функциональных покрытий, директор научно-учебного центра самораспространяющегося высокотемпературного синтеза
Университет науки и технологий МИСИС, Москва (Россия)

***E-mail: smukanov@misis.ru**

[1]ORCID: https://orcid.org/0000-0001-6719-6237
[2]ORCID: https://orcid.org/0000-0003-2505-2918
[3]ORCID: https://orcid.org/0000-0002-1736-8050
[4]ORCID: https://orcid.org/0000-0002-0623-0013

Поступила в редакцию 23.06.2023 *Принята к публикации 16.11.2023*

Аннотация: Неудовлетворительное качество поверхностного слоя аддитивных изделий, в частности повышенная шероховатость поверхности, препятствует широкому применению селективного электронно-лучевого сплавления (СЭЛС). Одним из способов выглаживания, а также упрочнения поверхностного слоя является электроискровая обработка (ЭИО). В работе показана возможность модифицирования поверхности аддитивных образцов из сплава ВТ6 путем реакционной ЭИО многокомпонентными электродами. Для этого были использованы электроды из объемноаморфизуемого сплава $Fe_{48}Cr_{15}Mo_{14}Y_2C_{15}B_6$ и высокоэнтропийного сплава $FeCoCrNi_2$. По результатам растровой электронной микроскопии установлено, что после ЭИО оба модифицированных слоя имеют толщину около 16 мкм. Рентгеноструктурный фазовый анализ показал, что в случае обработки аморфным электродом они содержат карбобориды типа Ti(B,C), а в случае обработки высокоэнтропийным электродом – интерметаллиды типа $Ti_2(Fe,Ni)$. Модифицированные слои имеют средние значения твердости 19 и 10 ГПа и модуля упругости 234 и 157 ГПа соответственно, что значительно превышает значения этих параметров для сплава ВТ6, выращенного СЭЛС. Электроискровое модифицирование поверхности многокомпонентными электродами привело к уменьшению шероховатости в 8…11 раз за счет оплавления выступов и заполнения впадин расплавом на глубину более 50 мкм. Сравнительный анализ результатов трибологических испытаний показал изменение механизма износа в результате ЭИО аддитивного сплава ВТ6. Износостойкость повысилась на 4 и 3 порядка величины при применении электродов из объемноаморфизуемого и высокоэнтропийного сплава соответственно.

Ключевые слова: титановый сплав; селективное электронно-лучевое сплавление; шероховатость поверхности; выглаживание; упрочнение; износостойкость; электроискровая обработка; объемноаморфизуемые сплавы; высокоэнтропийные сплавы.

Благодарности: Работа выполнена при финансовой поддержке Министерства науки и высшего образования Российской Федерации в рамках государственного задания в сфере науки (проект № 0718-2020-0034).

Статья подготовлена по материалам докладов участников XI Международной школы «Физическое материаловедение» (ШФМ-2023), Тольятти, 11–15 сентября 2023 года.

Для цитирования: Муканов С.К., Логинов П.А., Петржик М.И., Левашов Е.А. Электроискровое модифицирование поверхности аддитивного сплава ВТ6 высокоэнтропийным и аморфным электродами // Frontier Materials & Technologies. 2024. № 1. С. 49–60. DOI: 10.18323/2782-4039-2024-1-67-5.